Journal of Biomedical Optics

BiomedicalOptics.SPIEDigitalLibrary.org

Automated microaneurysm detection in diabetic retinopathy using curvelet transform

Syed Ayaz Ali Shah
Augustinus Laude
Ibrahima Faye
Tong Boon Tang

SPIE.

Automated microaneurysm detection in diabetic retinopathy using curvelet transform

Syed Ayaz Ali Shah,[a] Augustinus Laude,[b] Ibrahima Faye,[c] and Tong Boon Tang[a,*]
[a]Universiti Teknologi PETRONAS, Department of Electrical and Electronic Engineering, Centre for Intelligent Signal and Imaging Research, Bandar Seri Iskandar, Perak 32610, Malaysia
[b]National Healthcare Group Eye Institute, Tan Tock Seng Hospital, Singapore 308433, Singapore
[c]Universiti Teknologi PETRONAS, Department of Fundamental and Applied Sciences, Centre for Intelligent Signal and Imaging Research, Bandar Seri Iskandar, Perak 32610, Malaysia

Abstract. Microaneurysms (MAs) are known to be the early signs of diabetic retinopathy (DR). An automated MA detection system based on curvelet transform is proposed for color fundus image analysis. Candidates of MA were extracted in two parallel steps. In step one, blood vessels were removed from preprocessed green band image and preliminary MA candidates were selected by local thresholding technique. In step two, based on statistical features, the image background was estimated. The results from the two steps allowed us to identify preliminary MA candidates which were also present in the image foreground. A collection set of features was fed to a rule-based classifier to divide the candidates into MAs and non-MAs. The proposed system was tested with Retinopathy Online Challenge database. The automated system detected 162 MAs out of 336, thus achieved a sensitivity of 48.21% with 65 false positives per image. Counting MA is a means to measure the progression of DR. Hence, the proposed system may be deployed to monitor the progression of DR at early stage in population studies. [DOI: 10.1117/1.JBO.21.10.101404]

Keywords: diabetic retinopathy; microaneurysms; curvelet transform; fundus images.

Paper 150747SSR received Nov. 4, 2015; accepted for publication Jan. 18, 2016; published online Feb. 11, 2016.

1 Introduction

A majority of the people suffering from diabetes mellitus will eventually develop diabetic retinopathy (DR). At the final stage of DR, sufferers may lose their eyesight. DR is one of the leading causes of blindness and can be controlled if detected early. But for population-based assessment, the task of grading each retinal fundus image is both time consuming and labor intensive. With the advent of digital fundus photograph technology and the availability of fast computers, systems are being designed to detect DR automatically. Microaneurysms (MAs), which are basically the saccular enlargement of the venous ends of retinal capillaries, are said to be the first sign of DR. MAs appear and disappear during the early course of retinopathy.[1,2] The MA count and turnover in digital color fundus images are important measures of DR progression.[3,4] Therefore, accurately detecting MA is not only important for DR detection, but also it may assist in monitoring DR progression.

The MAs have diameters between 10 and 100 μm, are round in shape, and their color is similar to blood vessels (BVs) (red),[5,6] as shown in Fig. 1. Detection of MAs is challenging due to the variation in MA size, low and varying contrast, uneven illumination, and variation in fundus image background. MA detection is not a new topic; many researchers have worked on it since the early 1980s.[7,8] Though the performance of the automatic system in digitized fluorescein angiograms is somewhat on par with a human grader,[9] it is considered to be an invasive method, as fluorescein sodium dye is injected into the eye. The associated risk of complication or adverse reaction can include transient nausea, occasional vomiting, and so on, and in very rare cases can cause death. Thus most of the current research is moving toward color fundus photography, which is a noninvasive imaging method. In the absence of contrast enhancing agent, color fundus images inevitably suffer from low contrast. The performance of the fundus image-based system is, as expected, limited and remains as an open issue in retinal image analysis.

Some of the well-known approaches used in MA detection include template matching in wavelet domain, scale-adapted blob analysis with semisupervised learning scheme, ensemble-based system, double-ring filter, local rotating cross-section profile analysis, multiscale correlation coefficients, and pixel classification technique.[10–16] In this work, we propose to use curvelet transform (CT) for MA detection as it can detect curve singularities. Our preliminary work indicated promising results (Shah et al.[17] IOVS 2015;56: ARVO E-Abstract 5266).

2 Materials and Methods

2.1 *Data Description*

We tested our system using a publicly available Retinopathy Online Challenge (ROC) dataset.[18] The dataset consists of 50 images with ground truth at different resolutions mimicking the real-world scenario. The MAs were annotated by four eye specialists at the Department of Ophthalmology, University of Iowa. The ROC dataset is challenging due to the presence of noise, compression artifacts, and the general image quality. These are in common to the image quality found in mass screening projects. The images were acquired using different types of camera and at different resolutions, which makes it more difficult to detect MAs in such images. The fundus cameras used

*Address all correspondence to: Tong Boon Tang, E-mail: tongboon.tang@petronas.com.my

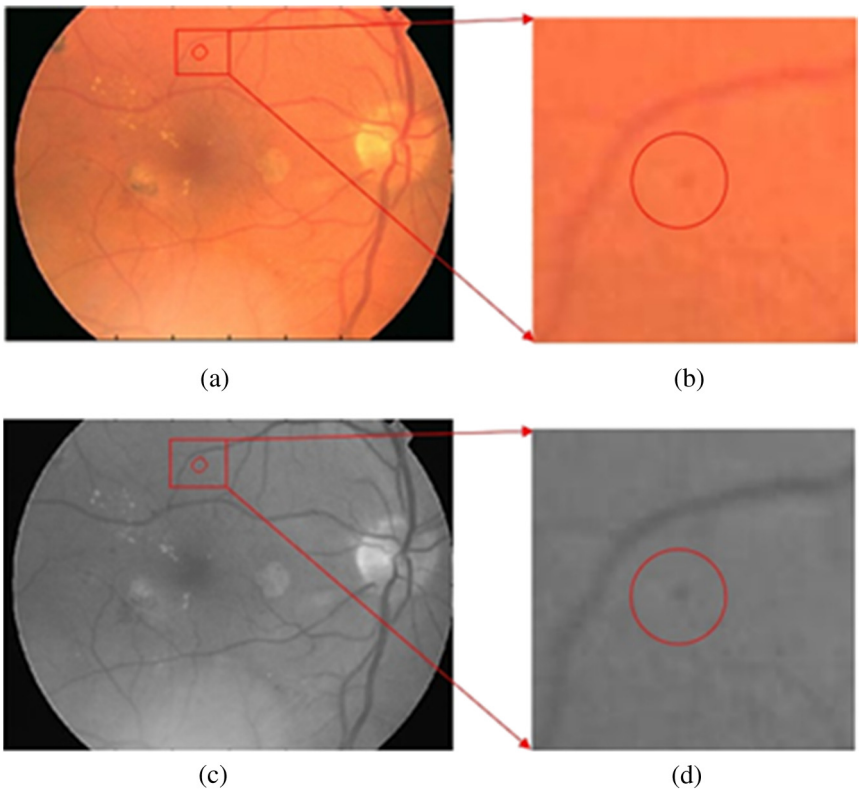

Fig. 1 Example of MA, where row 1 shows the MA in (a) full-color RGB and (b) a close-up view; row 2 is (c) in green band and (d) with a close-up view.

were Topcon NW 100, a Topcon NW200, and a Canon CR5-45NM. Niemeijer selected them from 150,000 photographs collected in a DR screening program to form the ROC dataset.[19] Table 1 describes the different image types.[18]

2.2 *Automated Microaneurysm Detection System*

Figure 2 depicts the complete procedure of the proposed MA detection system which consists of the following steps:

1. Candidate selection
   a. BV extraction from green band of raw image, preprocessing of green band, removal of BV from preprocessed green band, and MA candidate selection using local thresholding.
   b. Background estimation using gray band of raw image.
   c. Removal of candidates from step a that appear in the background.
2. Candidate features extraction
   a. Color-based features.
   b. Hessian-based features.
   c. Curvelet-based features.
3. Candidate classification

Since the dataset consists of different sizes of images, the height of all the images was resized to a standard 800-pixel while maintaining their original width/height ratio. After resizing, each color fundus image was divided into red band (G_r), green band (G_n), and gray band (G_y). We preprocessed the G_n by shade correction, followed by histogram equalization to obtain the preprocessed image denoted by G_{npr}. The BVs were extracted from the G_n, using two-dimensional (2-D) Gabor wavelet,[20] and removed from the G_{npr} to obtain BV-removed image denoted by G_{-BV}. The MA candidates were obtained in two parallel steps, namely local thresholding and statistical features-based technique. The MAs have low intensity in green band. Using local thresholding,[21] MA candidate pixels with low intensities could be selected from G_{-BV} as potential candidates. Also from the gray band image (G_y), based on pixel contrast and standard deviation, we could identify MA candidates. Only those candidates which were found by both of these methods were retained. In both MA candidate

Table 1 Types of images used in the proposed approach.

	Resolution (height × width in pixels)	Coverage of the retina	Number of images
Type I	768 × 576	45 deg	22
Type II	1058 × 1061	45 deg	3
Type III	1389 × 1383	45 deg	25

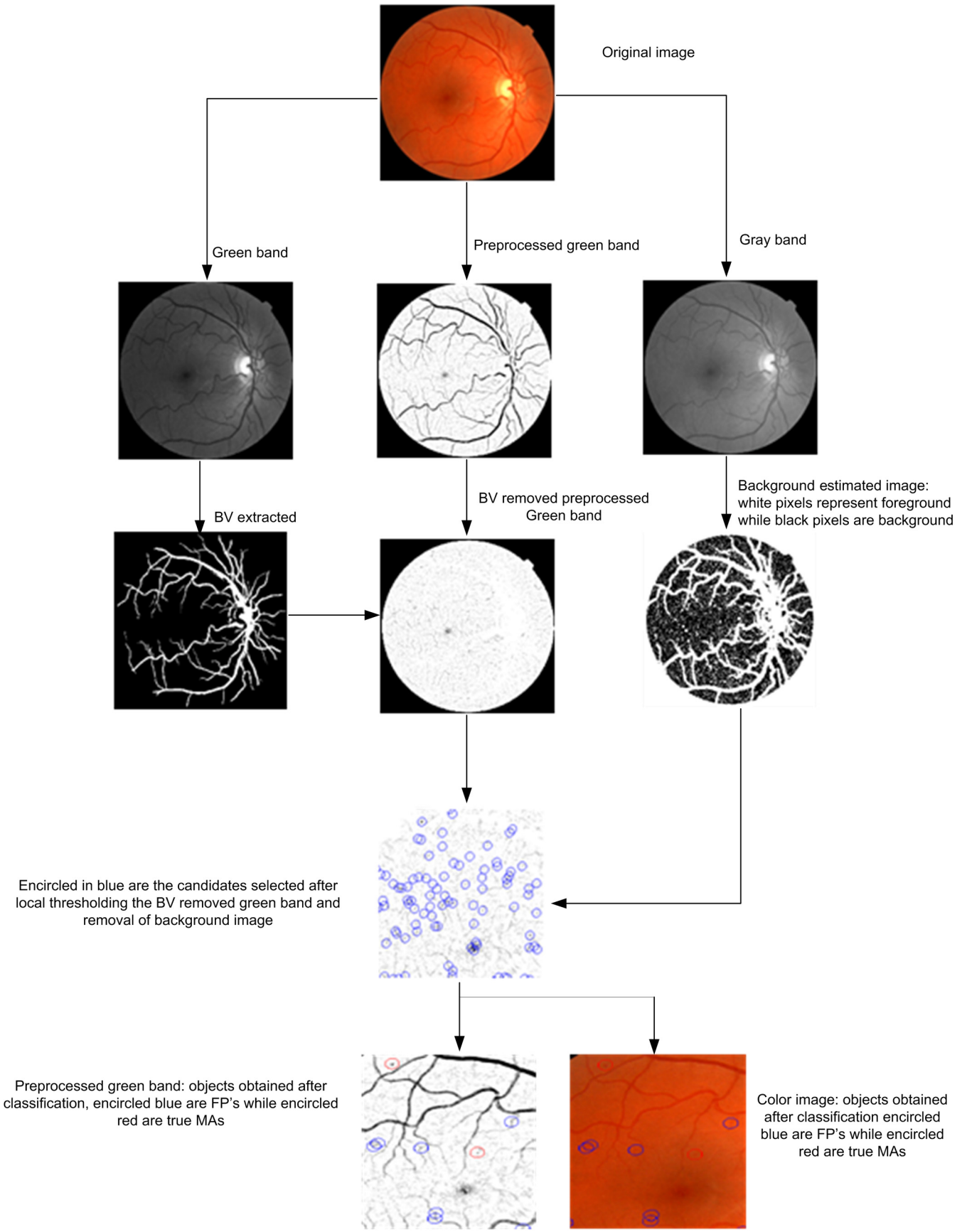

Fig. 2 Automated MAs detection system flowchart.

selections, thresholds were kept at low value to maximize the detection of MAs. Hence, many true MAs were detected along with hundreds of false positives (FPs). These FPs were mainly from the traces of the BVs, the background and bits of larger red lesions.

2.3 *Candidate Feature Extraction*

In general, MAs are red in color and have round shape. Based on their morphology and intensity, we used three feature sets to describe the MAs, namely color-based, Hessian matrix-based, and curvelet coefficients-based features. The color features include (a) standard deviation and mean intensity values in red and green bands, and (b) the histogram of S and V bands in HSV color space. The BVs and other linear objects can be detected based on the eigenvalues of Hessian matrix.[22] The features we used based on Hessian matrix are thus the eigenvalues, their product, and their ratio.

The basic concept of curvelets[23] is to represent a curve as a superposition of multiple functions of various lengths and widths obeying the scaling law width $\approx$ length^2. CT has a highly redundant dictionary, which can provide sparse representation of signals that have edges along regular curve. It is localized in angular orientation in addition to localization in spatial and frequency domains—a very important feature missing in the classic wavelet transform. Initial construction of curvelets has been redesigned and was reintroduced as fast digital CT.[24]

Curvelets are used in many medical image analysis applications like computed tomography,[25] breast cancer diagnosis in digital mammogram,[26] ulcer detection,[27] retinal image analysis,[28] and so on. Most natural images/signals exhibit line-like edges, i.e., discontinuities across curves (so-called line or curve singularities). Traditional wavelets perform well only at representing point singularities, since they ignore the geometric properties of structures and do not exploit the regularity of edges.[29] The solution to this problem and some other limitations of the wavelet was provided by CT.[23] Unlike the isotropic elements of wavelets, the needle-shaped elements of this transform possess very high directional sensitivity and anisotropy.[29] The algorithm of CT is shown in Fig. 3. It is based on two windows, namely scale window V and radial window W, and consists of four steps: (a) compute the 2-D Fourier transform of the original image, and (b) for each scale s and orientation n, estimate frequency window $U_{s,n}$ as a product of the scale and radial windows, (c) wrap this product around the origin, and (d) compute a 2-D inverse fast Fourier transform to derive the curvelet coefficients. More details can be found in Candes' paper.[24] In digital implementation of the CT, the two main parameters are

a. number of scales and
b. number of orientations

at the coarsest level. We found in our case that 2 scales and 16 orientations work well. Based on curvelet coefficients, we calculated aspect ratio, circulatory, mean energy, and standard deviation of energy.

2.4 *Candidate Classification*

A simple rule-based classifier was designed to classify the candidates into MA and non-MA. The classification was done in three sequential stages. In stage one, using color features we removed the FPs. In stage two, using Hessian matrix-based features we removed those candidates that were from traces of BVs and other elongated objects. While in stage three, we utilized the curvelet coefficients-based features to remove non-circular objects.

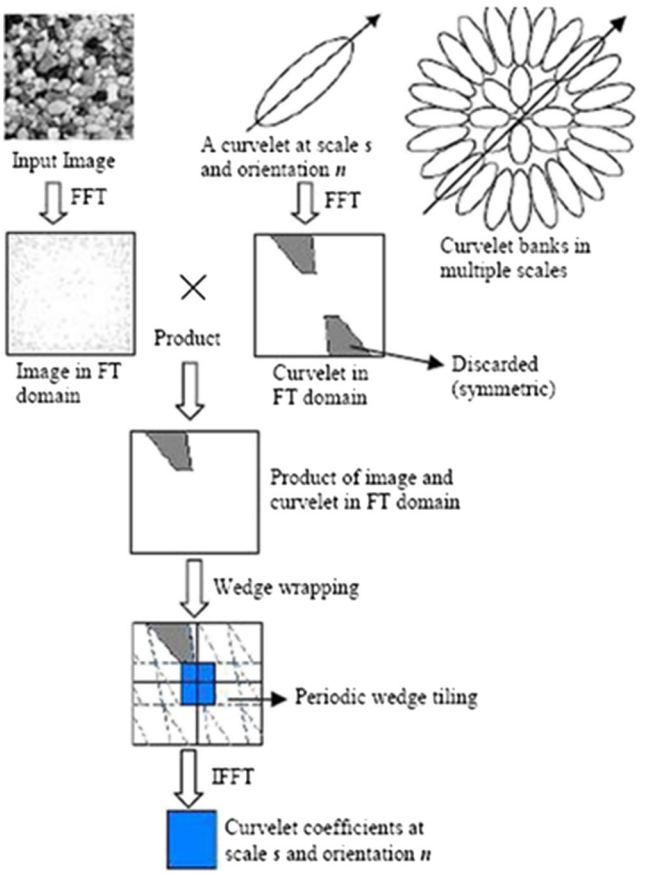

Fig. 3 Steps of CT.[28]

3 Results and Discussion

Out of the 50 images, only 37 images contain MAs, while the remaining 13 images do not contain any MA. The total number of MAs in these 37 images is 336. The results of the proposed system and those previously reported in literature are shown in Table 2. Out of the 336 MAs, the proposed approach was able to detect 162 MAs, achieving a sensitivity of 48.21% with 65 FPs per image (FPPI). This result is favorably comparable with the

Table 2 Result comparison of different MA detection methods.

References	Methodology	Sensitivity (%)	FPPI
Spencer et al.[30]	Top-hat transform	12.00	20.30
Abdelazeem[31]	Circular Hough transform	28.00	505.85
Walter et al.[32]	Diameter closing	36.00	154.42
Zhang et al.[15]	Multiple-Gaussian mask	33.00	328.30
Lazar et al.[14,33]	Cross-section profile	48.00	73.94
Adal et al.[11]	Hessian operator	44.64	35.20
Our method	CT	48.21	65.00

state-of-the-arts, although only simple rule-based classifier was implemented. Unlike the method by Adal et al. that employed four supervised classifiers and 87 features in total to select an optimum classifier–feature pairing to remove FPs, the computation of the proposed system is simpler and faster albeit at the expense of higher FPPI. In this work, we aimed to achieve high sensitivity in MA detection, i.e., to detect as many MAs as possible from fundus images. We used local thresholding technique in identifying MA candidates and kept the threshold to a low value as our approach to achieve maximum possible sensitivity, at the cost of hundreds of FPPI. These FPs at this initial stage were mainly due to background of the fundus images and BVs. We used statistical features to estimate the background and remove those candidates that are from background. In addition, during the BV extraction stage, we kept the threshold to a low value so that only true BVs are extracted. This helps us in detecting MAs near the BV and ultimately improving the sensitivity. However, this resulted in introducing many FPs as there were many traces of BVs. To eliminate those BVs, we used the Hessian matrix-based features. Thus, the proposed system can detect MA near the BVs with reasonably good specificity. Figure 4 illustrates the examples of MA detected in close vicinity to BVs.

As previously mentioned, our objectives are different, in that we have targeted for better sensitivity whereas they focused on specificity. As the "good" MAs (clear circular dark red spots) form only a fraction of all the MAs in this dataset, this has a significant impact on how robust one approach can be optimized in coping with the variance of MA features. Using larger number of features and more complex classifiers, Adal et al. were successful in achieving very good specificity. Increasing its sensitivity (i.e., accepting MAs with larger variance) may however not be straightforward.

Figure 5 shows the free-response receiver operating characteristic (FROC) curve of the proposed system. Based on local thresholding alone, the proposed system would have hundreds of FPPI. More than 42% of those FPs could however be removed using color features, with only 2.3% of the MAs being lost. We started with 178 MAs detected out of possible 336 (with 250 FPPI), after local thresholding. The results

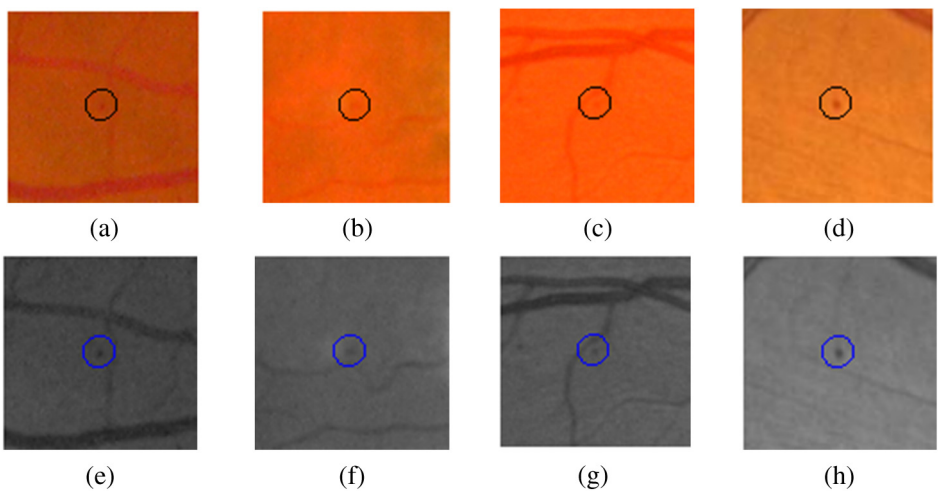

Fig. 4 Examples of MA that are very close to the BVs but detected by the proposed system: (a)–(d) full-color images and (e)–(h) in green band.

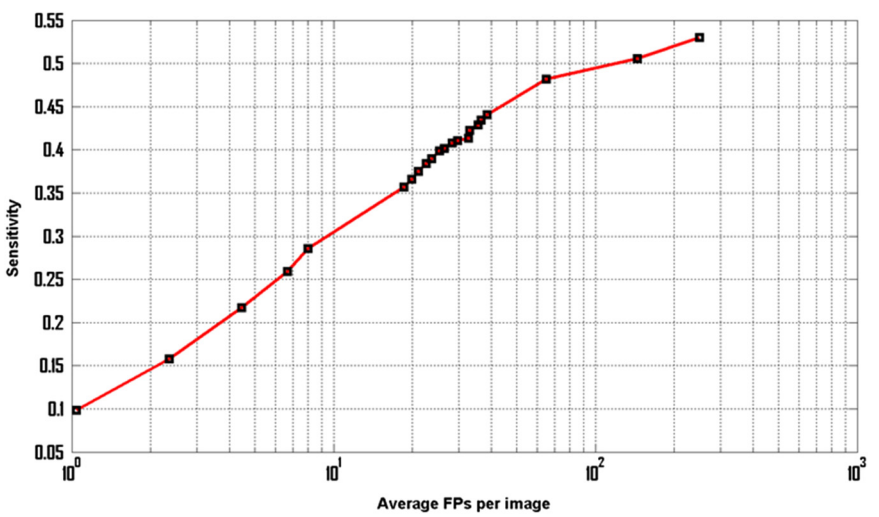

Fig. 5 FROC plot of the proposed system.

were improved to 170 MAs with 144 FPPI, after MA candidate selection based on color features. However, to achieve very high specificity (<100 FPPI), additional features are required to differentiate the actual MAs and the FPs. In this case, we optimized the results using Hessian and curvelet features simultaneously.

To our best knowledge, CT is used for the first time in MA detection. CT is fast and robust at detecting objects with curved singularities. We used features including shape parameters based on curvelet coefficients to discriminate between MAs and non-MAs. The results indicate that curvelets are very effective at detecting round objects such as MAs. Table 2 further shows our approach achieves the higher sensitivity than other reported approaches. Admittedly, the FPPI is higher than Adal's but a simpler solution is perhaps better, as the Occam's razor principle suggests.

The ROC dataset is a very challenging dataset. It has been observed that general image quality, noise, and low and varying contrast make it difficult to detect MAs in this dataset. Figure 6 depicts some of the MA candidates detected by the proposed system. The FPs are mostly from BVs and hemorrhages (large red lesions). Some of the images are very dark, hence in those images the background has also contributed to the FPs. Factors such as variation in fundus image background, low and varying contrast, and artifact are found to further limit the MA detection rate. The cases where the proposed system failed to detect MAs are shown in Fig. 7 and can be summarized into three categories:

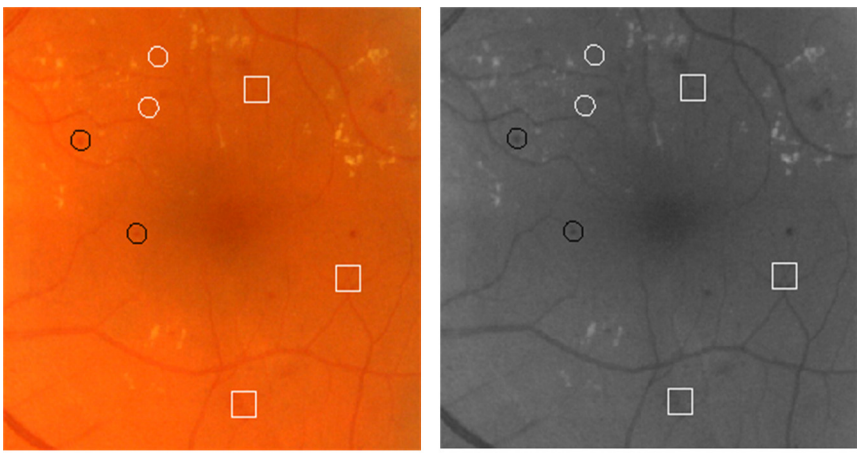

Fig. 6 Objects encircled in black are true positives, encircled in white are false negatives, whereas objects inside the white squares are FPs: (a) full-color image while (b) in green band.

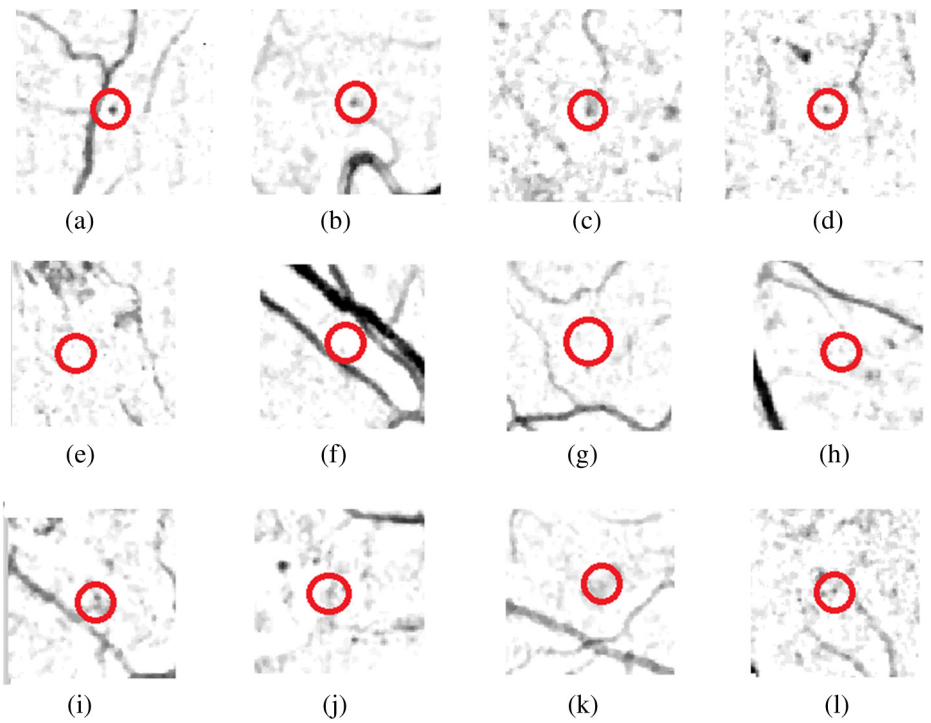

Fig. 7 Different cases where the proposed system was unable to detect the MAs: (a)–(d) examples of missed MA because the center pixel does not have the minimum intensity, (e)–(h) examples of missed MA because their colors are very faint, and (i)–(l) examples of missed MA due to abnormal shape.

Case I: If the central pixel of the MA is not the darkest point, then in some cases that MA will be missed. The hit criteria specified by ROC[18] are very strict. We assumed that the center point of the MA to be the darkest point. But in some cases, the ground truth does not represent the darkest point. In such cases, if the darkest point of the detected lesion is not within the specified distance from the ground truth, then it is declared as missed.

Case II: All those MAs which are very faint in color will be missed, as the candidates are extracted based on the assumption that MAs have low intensity in green band, i.e., dark in color as intensity level increases from dark/black (value = 0) to faint/white (value = 255). Thus, those MAs which are faint in color, i.e., having very high intensity value in green band, will be missed. These are the examples of MAs which were missed in the first stage. Most of the missed MAs belong to this category.

Case III: Those MAs having abnormal shape will also be missed, since the proposed algorithm assumes MAs to be somehow round in shape. So all those MAs selected at the initial stage will be missed in the final stage of classification if they have noncircular shape.

One possible approach to improve the sensitivity and specificity of the proposed MA detection system is the utilization of multispectral imaging (MSI) approach. Applications of MSI have shown promising results in different areas of biomedical image analysis ranging from human forearm imaging to skin chromophore mapping,[34–38] with several applied to retinal image analysis.[39–42] A recent study on retinal vein occlusion demonstrated that MSI was able to define vascular abnormalities at a comparable performance as fundus photography, fundus fluorescein angiography, and optical coherence tomography.[43] In MSI, image data are captured at specific nonoverlapping frequency bands. Thus, certain features within the field of view can be highlighted. If applied in MA detection, we expect better BV extraction and background separation may be achieved. These will result in less stringent requirement at the classifier stage, and hence improvement in sensitivity.

4 Conclusion

We have explored a new technique for MA detection. We observed that the main sources/contributors of FPs in automated MA detection such as proposed one are image background and BVs while hemorrhages are the third category of FPs although with fewer in numbers. The proposed system has a high sensitivity and is able to detect MAs near the BVs. Our future work includes investigation of a means to detect hemorrhages and fine BVs to further improve the specificity of our proposed MA detection system.

Acknowledgments

The project was supported by National Healthcare Group Singapore (Grant No. NHG/CSCS/12006). S. A. A. Shah was a recipient of Universiti Teknologi PETRONAS graduate assistantship scheme.

References

1. T. Hellstedt and I. Immonen, "Disappearance and formation rates of microaneurysms in early diabetic retinopathy," *Br. J. Ophthalmol.* **80**(2), 135–139 (1996).
2. E. Kohner et al., "Microaneurysms in the development of diabetic retinopathy (UKPDS 42)," *Diabetologia* **42**(9), 1107–1112 (1999).
3. R. Klein et al., "Retinal microaneurysm counts and 10-year progression of diabetic retinopathy," *Arch. Ophthalmol.* **113**(11), 1386–1391 (1995).
4. L. Ribeiro, S. Nunes, and J. Cunha-Vaz, "Microaneurysm turnover in the macula is a biomarker for development of clinically significant macular edema in type 2 diabetes," *Curr. Biomarker Find.* **3**, 11–15 (2013).
5. T. Walter and J.-C. Klein, "Automatic detection of microaneurysms in color fundus images of the human retina by means of the bounding box closing," in *Medical Data Analysis*, A. Colosimo, P. Sirabella, and A. Giuliani, Eds., pp. 210–220, Springer, Berlin-Heidelberg, Germany (2002).
6. A. W. Fryczkowski et al., "Scanning electron microscopic study of microaneurysms in the diabetic retina," *Ann. Ophthalmol.* **23**(4), 130–136 (1991).
7. B. Lay, C. Baudoin, and J.-C. Klein, "Automatic detection of microaneurysms in retinopathy fluoro-angiogram," in *27th Annual Technical Symp.*, pp. 165–173 (1984).
8. C. Baudoin, B. Lay, and J. Klein, "Automatic detection of microaneurysms in diabetic fluorescein angiography," *Rev. Epidemiol. Sante Publique* **32**(3–4), 254–261 (1984).
9. J. V. Forrester, "A fully automated comparative microaneurysm digital detection system," *Eye* **11**, 622–628 (1997).
10. G. Quellec et al., "Optimal wavelet transform for the detection of microaneurysms in retina photographs," *IEEE Trans. Med. Imaging* **27**(9), 1230–1241 (2008).
11. K. M. Adal et al., "Automated detection of microaneurysms using scale-adapted blob analysis and semi-supervised learning," *Comput. Methods Programs Biomed.* **114**(1), 1–10 (2014).
12. B. Antal and A. Hajdu, "An ensemble-based system for microaneurysm detection and diabetic retinopathy grading," *IEEE Trans. Biomed. Eng.* **59**(6), 1720–1726 (2012).
13. A. Mizutani et al., "Automated microaneurysm detection method based on double ring filter in retinal fundus images," *Proc. SPIE* **7260**, 72601N (2009).
14. I. Lazar and A. Hajdu, "Retinal microaneurysm detection through local rotating cross-section profile analysis," *IEEE Trans. Med. Imaging* **32**(2), 400–407 (2013).
15. B. Zhang et al., "Detection of microaneurysms using multi-scale correlation coefficients," *Pattern Recognit.* **43**(6), 2237–2248 (2010).
16. M. Niemeijer et al., "Automatic detection of red lesions in digital color fundus photographs," *IEEE Trans. Med. Imaging* **24**(5), 584–592 (2005).
17. A. S. Syed et al., "Automated detection of microaneurysms using curvelet transform," *Invest. Ophthal. Vis. Sci.* **56**(7), 5266 (2015).
18. M. Niemeijer et al., "Retinopathy online challenge: automatic detection of microaneurysms in digital color fundus photographs," *IEEE Trans. Med. Imaging* **29**(1), 185–195 (2010).
19. M. D. Abramoff and M. S. Suttorp-Schulten, "Web-based screening for diabetic retinopathy in a primary care population: the EyeCheck project," *Telemed. J. E Health* **11**(6), 668–674 (2005).
20. J. V. Soares et al., "Retinal vessel segmentation using the 2-D Gabor wavelet and supervised classification," *IEEE Trans. Med. Imaging* **25**(9), 1214–1222 (2006).
21. S. S. A. Ali et al., "Making every microaneurysm count: a hybrid approach to monitor progression of diabetic retinopathy," in *5th Int. Conf. on Intelligent and Advanced Systems (ICIAS)*, pp. 1–4 (2014).
22. A. F. Frangi et al., "Multiscale vessel enhancement filtering," in *Medical Image Computing and Computer-Assisted Interventation—MICCAI'98*, pp. 130–137, Springer (1998).
23. E. J. Candes and D. L. Donoho, "Curvelets: a surprisingly effective nonadaptive representation for objects with edges," DTIC Document, Technical Report ADP 11978 (2000).
24. E. Candes et al., "Fast discrete curvelet transforms," *Multiscale Model. Simul.* **5**(3), 861–899 (2006).
25. L. Dettori and L. Semler, "A comparison of wavelet, ridgelet, and curvelet-based texture classification algorithms in computed tomography," *Comput. Biol. Med.* **37**(4), 486–498 (2007).
26. M. M. Eltoukhy, I. Faye, and B. B. Samir, "Breast cancer diagnosis in digital mammogram using multiscale curvelet transform," *Comput. Med. Imaging Graphics* **34**(4), 269–276 (2010).
27. B. Li and M. Q.-H. Meng, "Texture analysis for ulcer detection in capsule endoscopy images," *Image Vision Comput.* **27**(9), 1336–1342 (2009).

28. M. S. Miri and A. Mahloojifar, "Retinal image analysis using curvelet transform and multistructure elements morphology by reconstruction," *IEEE Trans. Biomed. Eng.* **58**(5), 1183–1192 (2011).
29. J. Ma and G. Plonka, "The curvelet transform," *IEEE Signal Process. Mag.* **27**(2), 118–133 (2010).
30. T. Spencer et al., "Automated detection and quantification of microaneurysms in fluorescein angiograms," *Graefe's Arch. Clin. Exp. Ophthalmol.* **230**(1), 36–41 (1992).
31. S. Abdelazeem, "Micro-aneurysm detection using vessels removal and circular Hough transform," in *Proc. of the Nineteenth National Radio Science Conf. (NRSC 2002)*, pp. 421–426 (2002).
32. T. Walter et al., "Automatic detection of microaneurysms in color fundus images," *Med. Image Anal.* **11**(6), 555–566 (2007).
33. I. Lazar, A. Hajdu, and R. J. Quareshi, "Retinal microaneurysm detection based on intensity profile analysis," in *8th Int. Conf. on Applied Informatics*, pp. 157–165 (2010).
34. M. Ehler, "Modifications of iterative schemes used for curvature correction in noninvasive biomedical imaging," *J. Biomed. Opt.* **18**(10), 100503 (2013).
35. A. R. Rouse and A. F. Gmitro, "Multispectral imaging with a confocal microendoscope," *Opt. Lett.* **25**(23), 1708–1710 (2000).
36. C. Yuan et al., "In vivo accuracy of multispectral magnetic resonance imaging for identifying lipid-rich necrotic cores and intraplaque hemorrhage in advanced human carotid plaques," *Circulation* **104**(17), 2051–2056 (2001).
37. I. Kuzmina et al., "Towards noncontact skin melanoma selection by multispectral imaging analysis," *J. Biomed. Opt.* **16**(6), 060502 (2011).
38. J. M. Kainerstorfer et al., "Principal component model of multispectral data for near real-time skin chromophore mapping," *J. Biomed. Opt.* **15**(4), 046007 (2010).
39. M. Ehler et al., "Modeling photo-bleaching kinetics to create high resolution maps of rod rhodopsin in the human retina," *PLoS One* **10**(7), e0131881 (2015).
40. I. Styles et al., "Quantitative analysis of multi-spectral fundus images," *Med. Image Anal.* **10**(4), 578–597 (2006).
41. C. Zimmer et al., "Innovation in diagnostic retinal imaging: multispectral imaging," *Retina Today* **9**(7), 94–99 (2014).
42. W. Czaja and M. Ehler, "Schödinger eigenmaps for the analysis of bio-medical data," *IEEE Trans. Pattern Anal. Mach. Intell.* **35**(5), 1274–1280, (2013).
43. Y. Xu et al., "A light-emitting diode (LED)-based multispectral imaging system in evaluating retinal vein occlusion," *Lasers Surg. Med.* **47**(7), 549–558 (2015).

Syed Ayaz Ali Shah received his master degree in electrical engineering from NWFP University of Engineering and Technology Peshawar, Pakistan, in 2007. He is currently working toward the PhD degree at the Center of Intelligent Signal and Imaging Research (CISIR), Department of Electrical and Electronic Engineering, Universiti Teknologi PETRONAS, Malaysia. He is the recipient of PETRONAS graduate assistantship scheme. His research interest includes medical image analysis, image processing, pattern recognition and computer vision.

Augustinus Laude is head, research and a senior consultant of Ophthalmology in the National Healthcare Group Eye Institute at Tan Tock Seng Hospital. He received his MBChB degree from the University of Edinburgh, and completed his fellowship with the Royal College of Surgeon in Edinburgh and the Academy of Medicine Singapore. He is an adjunct assistant professor at Nanyang Technical University and Adjunct Clinician Scientist at Singapore Eye Research Institute. His clinical and research interests include cataract surgery, macula diseases and low vision.

Ibrahima Faye is an associate professor at Universiti Teknologi PETRONAS. His BSc, MSc and PhD degrees in mathematics are from University of Toulouse, France, while his MS degree in engineering of Medical and Biotechnological data is from Ecole Centrale Paris, France. His research interests include Engineering Mathematics, Signal and Image Processing, Pattern Recognition, and Dynamical Systems.

Tong Boon Tang is an associate professor of electrical & electronic engineering at the Universiti Teknologi PETRONAS. He received his PhD and BEng(Hons) degrees both from the University of Edinburgh. He is a recipient of IET Nanobiotechnology Premium Award and Lab on Chip Award. His research interests are in biomedical instrumentation, from device and measurement to data fusion. He is an associate editor of Journal of Medical Imaging and Health Informatics.